Tropical Warm Pool Surface Heat Budgets and Temperature: Contrasts Between 1997–98 El Nino and 1998–99 La Nina

Shu-Hsien Chou, Ming-Dah Chou

Laboratory for Atmospheres, NASA Goddard Space Flight Center

Greenbelt, Maryland

Pui-King Chan

Science Systems & Applications, Inc., Lanham, Maryland

Po-Hsiung Lin

National Taiwan University, Taipei, Taiwan

Kung-Hwa Wang

Central Weather Bureau, Taipei, Taiwan

Journal of Climate

January 27, 2003

Corresponding author: Dr. Shu-Hsien Chou, Code 912, Laboratory for Atmospheres, NASA Goddard Space Flight Center, Greenbelt, MD 20771.

E-mail: Shu-Hsien.Chou-1@nasa.gov

ABSTRACT

Seasonal and interannual variations of the net surface heating (F_{NET}) and sea surface temperature tendency (T_S/dt) in the tropical eastern Indian and western Pacific Oceans are studied. The surface heat fluxes are derived from the Special Sensor Microwave/Imager and Japanese Geostationary Meteorological Satellite radiance measurements for the period October 1997–September 2000. It is found that the magnitude of solar heating is lager than that of evaporative cooling, but the spatial variation of the latter is significantly large than the former. As a result, the spatial variations of seasonal and interannual variability of F_{NET} follow closely that of evaporative cooling. Seasonal variations of F_{NET} and T_S/dt are significantly correlated, except for the equatorial western Pacific. The high correlation is primarily attributable to high correlation between seasonal cycles of solar heating and T_S/dt.

The change of F_{NET} between 1997–98 El Nino and 1998–99 La Nina is significantly larger in the tropical eastern Indian Ocean than tropical western Pacific. For the former region, the reduced evaporative cooling arising from weakened winds during the El Nino is generally associated with enhanced solar heating due to decreased cloudiness, and thus increases the interannual variability of F_{NET}. For the latter region, the reduced evaporative cooling due to weakened winds is generally associated with but exceeds the reduced solar heating arising from increased cloudiness, and vise versa. Thus the interannual variability of F_{NET} is reduced due to this offsetting effect. Interannual variations of F_{NET} and T_S/dt have very low correlation. This is most likely related to interannual variability of ocean dynamics, which includes the variations of solar radiation penetrating through oceanic mixed layer, upwelling of cold thermocline water, Indonesian throughflow for transporting heat from the Pacific to Indian Ocean, and interhemispheric transport in the Indian Ocean.

1. Introduction

The warm pool of the tropical Indian and western Pacific Oceans is a climatic important region, which is characterized by the warmest sea surface temperature (SST), frequent heavy rainfall, strong atmospheric heating and weak mean winds with highly intermittent westerly wind bursts. The heating drives the global climate and plays the key role in the El Nino–Southern Oscillation (ENSO) and the Asian-Australian monsoon (Webster et al. 1998). Small changes in the SST of the Pacific warm pool associated with the eastward shift of the warm pool during the ENSO events have been shown to affect the global climate (Palmer and Mansfield 1984). Thus, the Tropical Ocean Global Atmosphere (TOGA) Coupled Ocean-Atmosphere Response Experiment (COARE) was conducted with the aim to better understand various physical processes responsible for the SST variation in the western Pacific warm pool (e.g., Andersonet al. 1996; Sui et al. 1997; Godfrey et al. 1998; Chou et al. 2000; and others).

One of the strongest El Nino warm events took place in the tropical Pacific Ocean, with a record-breaking SST warming occurred in the entire Indian Ocean during 1997–1998 (Yu and Rienecker 2000; Bell et al. 1999). The SST was observed to have negative (positive) anomalies in the eastern (western) equatorial Indian Ocean, which were referred to as Indian Ocean dipole mode and were large enough to reverse the climatological equatorial SST gradient. The relationships between the dipole mode and ENSO and Indian Ocean climate system have been extensively investigated (e.g., Webster et al. 1999; Saji et al. 1999; Yu and Riennecker 2000; and others).

Surface radiative and turbulent heat fluxes undergo large changes associated with seasonal and interannual variations of oceanic and atmospheric circulations. Although the surface heating is primarily determined by SST, clouds, and winds, it also has a large impact on the oceanic and atmospheric circulations. The purpose of this study is to provide information on seasonal and interannual variations of the surface heat budgets and the correlation of the surface heating with the rate of SST change in the tropical eastern Indian and western Pacific Oceans. This information is important for understanding the physical processes involving the interrelation, or feedback, between surface heating and the oceanic and atmospheric circulations.

Limited by the surface heat fluxes that we have computed using satellite radiance measurements, this study covers a 3-yr period of October 1997–September 2000 and the domain of 30°S–30°N, 90°E–170°W. This period covers the strong 1997–998 El Nino and the 1998–99 moderate La Nina (Bell et al. 1999, 2000). The annual-mean, seasonal and interannual variations of the surface heat fluxes during the 3-yr period are studied. In section 2, we briefly describe the data used, as well as the methods for deriving the surface fluxes and the retrieval accuracy. Section 3 presents the spatial distributions of annual-mean surface heat fluxes and some relevant parameters used for deriving the surface fluxes. Section 4 discusses the seasonal variation of surface heat fluxes and the SST tendency. Section 5 compares the surface heat fluxes, SST tendency, SST, clouds, surface wind speed and zonal wind stress between the 1997–98 El Nino and 1998–99 La Nina. Conclusions are given in Section 6.

2. Data sources, retrieval of surface fluxes and collocation validation

a. Data sources and retrieval of surface fluxes

The data used are 1°x1° lat–long monthly mean surface radiative and turbulent fluxes, SST, outgoing longwave radiation (OLR), and surface wind speed during the 3-yr period October 1997–September 2000. The radiative and turbulent fluxes are taken from the Goddard Satellite-retrieved Surface Radiation Budget (GSSRB; Chou et al. 2001) and Version 2 Goddard Satellite-based Surface Turbulent Fluxes (GSSTF2; Chou et al. 2002). The SST is taken from the NCEP/NCAR reanalysis (Kalney et al. 1996). Deep convection is inferred from the OLR of NOAA polar-orbiting satellites. The surface (10-m) wind speed is derived from the Special Sensor Microwave/Imager (SSM/I) radiance measurements (Wentz, 1997).

The GSSRB is retrieved empirically from the Japanese Geostationary Meteorological Satellite 5 (GMS-5) measurements of albedo in the visible channel and the brightness temperature in the 11–μm channel (Chou et al. 2001). The GSSRB covers a domain of 40°S–40°N, 90°E–170°W and a period of October 1997–December 2000. The spatial resolution is 0.5° x 0.5° lat-long, and the temporal resolution is 1 day. Compared to the observations at the Atmospheric Radiation Measurement (ARM) site on Manus Island (2.06°S, 147.43°E) during January 1998–June 2000,

the retrieved daily-mean downward surface solar (shortwave) flux has a positive bias of 6.2 W m^{-2} and a standard deviation (SD) error of 28.4 W m^{-2}; the retrieved daily-mean downward surface thermal infrared (longwave) flux has a positive bias of 1.9 W m^{-2} and a SD error of 6.6 W m^{-2}. These biases have been subtracted from the satellite retrievals in this study. Assuming errors of the retrieved daily fluxes are independent, the SD errors for the monthly-mean downward solar and infrared fluxes reduce to 5.2 W m^{-2} and 1.2 W m^{-2}, respectively.

The GSSTF2 is derived from the SSM/I radiance measurements over the global oceans (Chou et al. 2002). The GSSTF2 has a spatial resolution of 1° x 1° lat–long and covers the period July 1987–December 2000. Daily turbulent fluxes are derived from the SSM/I-inferred surface air humidity (Chou et al. 1995, 1997), SSM/I surface winds (Wentz 1997), and SST and 2-m air temperature of NCEP/NCAR reanalysis. The retrieval uses the algorithm of Chou et al. (1997) with adjustments of the salinity effect and the von Karmen constant. To include the salinity effect, the sea surface specific humidity (Q_s) is set to be 98% of the saturation humidity for pure water. In addition, the same von Karmen constant of 0.4 is used for velocity, temperature, and humidity following Fairall et al. (1996). The directions of wind stress are taken from those of the surface winds, which are derived from a blend of the SSM/I surface wind speeds (Wentz 1997), surface wind vectors from ships, buoys, and NCEP/NCAR reanalysis following the method of Atlas et al. (1996).

b. Collocation validation of GSSTF-2

Chou et al. (2002) validated the GSSTF2 bulk flux model, input variables and turbulent fluxes, based on ten field experiments conducted by the NOAA/Environmental Technology Laboratory (ETL) research ships. They also showed that the global distributions of 1988–2000 annual- and seasonal-mean turbulent fluxes had reasonable patterns related to the atmospheric general circulation and seasonal variations. In addition, they found that the GSSTF2 latent heat flux, surface air humidity, and winds are quite realistic compared to four other flux datasets. These four other datasets are GSSTF1 (version 1), HOAPS (Hamburg Ocean Atmosphere Parameters and Fluxes from Satellite Data), NCEP/NCAR reanalysis, and da Silva et al. (1994).

For conveniences, we present the collocation validation of the turbulent fluxes and input variables with the 1992–99 five tropical field experiments of NOAA/ETL research ships (Tables 1 and 2). Table 1 shows the periods and locations of the five tropical experiments: the Atlantic Stratocumulus Transition Experiment (ASTEX), the Coupled Ocean–Atmosphere Response Experiment (COARE; Fairall et al. 1996), the Joint Air–Sea Monsoon Interaction Experiment (JASMINE; Webster et al. 2002), the Kwajalein Experiment (KWAJEX), and the Nauru '99 (NAURU99). These five experiments provide hourly latent heat (F_{LH}) and sensible heat fluxes (F_{SH}) derived using the eddy correlation method. The experiments also provide hourly wind stresses determined using the inertial-dissipation (ID) method. Wind stress derived from the ID method is more accurate than that derived from the eddy correlation method for ship measurements (Fairall et al. 1996).

Table 2 compares the GSSTF2 daily-mean turbulent fluxes and input variables with those of the five field experiments. Compared to 134 daily turbulent fluxes of the five experiments, daily F_{LH} of GSSTF2 has a negative bias of –2.6 W m^{-2}, and a SD error of 29.7 W m^{-2}, and a correlation of 0.80. Daily F_{SH} has a positive bias of 7.0 W m^{-2} and a SD error of 6.2 W m^{-2}, and a correlation of 0.45. Daily wind stress has a positive bias of 0.0053 N m^{-2} and a SD error of 0.0193 N m^{-2}, and a correlation of 0.81. The positive bias of the F_{SH} is mainly due to the negative bias (–0.83°C) of surface air temperature of the NCEP/NCAR reanalysis in the tropical oceans. Noted that the retrieval-ship differences in daily turbulent fluxes include the spatial-temporal mismatch between GSSTF2 and ships, as well as the errors in the input variables and fluxes for both GSSTF2 and ship observations. The collocated daily variables of GSSTF2 are computed from 2 or 3 satellite observations averaged over an 1° area that encloses the ship locations, while those of the ships are computed from at least two hourly measurements over a much smaller area. Assuming daily retrieval errors are independent, the SD errors for the monthly-mean F_{LH}, F_{SH} and wind stress reduce to 5.4 W m^{-2}, 1.1 W m^{-2}, and 0.0035 N m^{-2}, respectively.

3. Annual mean

The downward net heat flux, F_{NET}, at the surface is defined as

$$F_{NET} = F_{SW} - (F_{LW} + F_{LH} + F_{SH}), \quad (1)$$

where F_{SW} is the net downward shortwave flux (solar heating), F_{LW} is the net upward longwave flux (IR cooling), F_{LH} is the upward latent heat flux (evaporative cooling), and F_{SH} is the upward sensible heat flux. The spatial distributions of F_{SW}, F_{LW}, F_{LH}, and F_{NET} averaged over October 1997–September 2000 for the domain 30°S–30°N, 90°E–170°W are shown in Fig.1. The period October 1997–May 1998 is part of the 1997–1998 El Nino, while June 1998–September 2000 is part of the 1998–2000 La Nina (Bell et al. 1999, 2000). Thus, the mean conditions for the 3-yr period of October 1997–September 2000 are generally closer to the long-term mean situations. The F_{SH} is generally very small (~5–15 W m^{-2}) and is not shown. Ranges of the annual-mean F_{SW}, F_{LW}, and F_{LH} are ~ 180–250, 50–70, and 75–190 W m^{-2}, respectively. Among the heat flux components, F_{SW} has the largest magnitude, and F_{LH} has the largest spatial variation. The spatial variation of F_{LW} is very small. As a result, the pattern of the spatial distribution of F_{NET} follows closely that of F_{LH}. For the annual mean condition within ~10–15° of the equator, the oceans gain heat up to ~ 75 W m^{-2}, due to the large solar heating and small evaporative cooling. Poleward of this region, the loss of heat by the ocean increases with latitudes primarily due to the increase in evaporative cooling.

The spatial distributions of the parameters relevant to the surface fluxes averaged over the 3-yr period are shown in Fig. 2. The deep cumulus cloudiness, usually indicated by OLR< 240 W m^{-2}, occurs in the maritime continent, the intertropical convergence zone (ITCZ; centered at ~7°N), and the southern Pacific convergence zone (SPCZ; centered at ~10°S) (Fig. 2a). Generally, the spatial distribution of solar heating (Fig. 1a) follows that of clouds, but with a smaller variability, reflecting the fact that solar heating depends not only on clouds but also on the seasonal and latitudinal variations of insolation at the top of the atmosphere. The SST contour of 29 °C embraces a large equatorial region west of the dateline (Fig. 2b). The IR cooling depends on clouds, SST, and the temperature and humidity of the atmospheric boundary layer. Although the range of the IR cooling is small (Fig. 1b), its spatial distribution resembles closely to that of clouds or OLR. Figure 2c shows that sea-air humidity difference (Q_s–Q_a) is large ~5–6 g kg^{-1}, but the spatial variability is

small. On the other hand, the spatial variation of the annual-mean surface wind speed is large, by a factor of two (4–9 m s^{-1}; Fig. 2d). The surface wind speed has a minimum in the equatorial convergence region and a maximum in the trade-wind regions. Thus, the evaporative cooling (Fig. 1c) follows primarily wind speed and secondarily Q_s–Q_a. The minimum evaporative cooling at the maritime continent coincides with the minimum in wind speed and Q_s–Q_a, whereas the maximum occurs in the trade-wind regimes, where the wind speed and Q_s–Q_a are both large.

We have compared the spatial distributions of the 3-yr mean turbulent fluxes with those averaged over the 13-yr period of 1988–2000 from GSSTF-2. It is found that the results are essential the same for the region under study, except that the 3–yr mean F_{LH} over the trade wind regions is larger by ~5–20 W m^{-2}. This is due to a slightly higher wind speed (~0.5 m s^{-1}) and sea-air humidity difference (~0.5 g kg^{-1}) in the regions. The spatial distributions shown in Fig. 1 are also found to be generally consistent with those of Oberhuber (1988), which were derived from the comprehensive ocean-atmosphere data set (COADS) covering the period 1950–79 with the data mainly from merchant ship's observations. Compared to Oberhuber (1988), however, F_{SW} is larger by ~25–40 W m^{-2}, F_{LW} is larger by ~10 W m^{-2}, F_{LH} in the trade-wind regions is larger by up to ~25 W m^{-2}, and F_{SH} is larger by ~5 W m^{-2}. Generally, the oceans gain more heat by up to ~30 W m^{-2} in the equatorial region, but lose more heat by a maximum of ~30 W m^{-2} in the South Indian Ocean trade-wind region. Kubota et al. (2002) compared the surface heat budgets of their Japanese Ocean Flux datasets with Use of Remote sensing Observations (J-OFURO) with those of da Silva (1994), which were also derived from COADS, for January and July 1993. They found that their F_{SW} and F_{LH} were generally larger than that of da Silva (1994) based on the COADS data. Their finding is consistent with our results.

4. Seasonal variations

Seasonal variations of F_{NET} and SST tendency (dT_S/dt) over the tropical eastern Indian and western Pacific Oceans are investigated for the boreal winter (December, January, February; DJF), spring (March, April, May; MAM), summer (June, July, and August; JJA), and fall (September, October, November; SON) of the 3-yr period October 1997–September 2000. Figure 3 shows the

seasonal-mean F_{NET}. The ITCZ follows the Sun to the summer hemisphere, and the trade winds are stronger in the winter hemisphere than in the summer hemisphere. The weak solar heating and the strong evaporative cooling cause a strong wintertime cooling of the ocean. On the contrary, the weak evaporative cooling and strong solar heating cause a strong summertime heating. The contrast between summertime heating and wintertime cooling is very large, ~150 W m^{-2} at 20° latitude in both hemispheres (Figs. 3a and 3c).

During spring and fall, insolation at the top of the atmosphere is a maximum in the equatorial region and the ITCZ is close to the equator. One would expect that the net surface heating decreases poleward due to a reduced solar heating and an enhanced evaporative cooling. However, F_{NET} is not symmetric about the equator. In the boreal spring (Fig. 3b), there is a broad band of strong surface heating extending from the northeast Indian Ocean northeastward to the northwestern side of the North Pacific high pressure region. The evaporative cooling in this band is much weaker than in the region to the east, which is in the strong trade-wind domain (not shown). The zonal contrast of F_{LH} reaches 120 W m^{-2} at 10°N. On the other hand, the zonal contrast of F_{SW} is much smaller, ~20 W m^{-2} (not shown). In the boreal fall, the southeastern Indian Ocean west of Australia has a strong net surface cooling (Fig. 3d). This strong surface cooling is due to strong winds associated with the Indian summer monsoon circulation. The contrast of F_{LH} between the regions east and west of Australia is ~80 W m^{-2}. In comparison, the zonal contrast of F_{SW} is only ~ 30 W m^{-2}.

Figure 4 shows the seasonal dT_S/dt averaged over the same 3-yr period. The SST increases during the spring and summer of both hemispheres but decreases during the fall and winter, except for the equatorial region. The magnitude of dT_S/dt increases poleward as the seasonal variation of SST increases poleward. The seasonal variation of dT_S/dt is larger in the Northern Hemisphere than in the Southern Hemisphere, which is consistent with the seasonal variation of F_{NET} (Fig. 3).

Figure 5 shows the correlation coefficient, r, of monthly dT_S/dt and F_{NET}, F_{SW}, and $-F_{LH}$ for the 3-yr period. Also shown in the figure are the regions that the correlation is significant at a 95% level (dark shaded). To determine the significance of the correlation, the standard deviation of the

correlation coefficient, SD, is derived following the approach of Lau and Chan (1983). The correlation is considered significant if r > 2SD, which has a 95% confidence level. It is found that regions of r > 2SD generally coincide with regions of r > 0.5–0.6 for all the three cases of correlation shown in the figure. Figure 5a shows that the correlation between monthly dT_S/dt and F_{NET} increases poleward and is generally very high, r ~ 0.8–0.9 poleward of 15–20° latitude. The correlation is generally lower, r ~ 0.4–0.6, for the western Pacific within ~10° of the equator. Thus, the seasonal variations of dT_S/dt and F_{NET} are significantly correlated at a confidence level of ~95%, except for some small areas in the equatorial western Pacific. For the North Indian Ocean, Loschnigg and Webster (2000) found that the seasonal variation of ocean heat storage was nearly balanced by that of the oceanic heat transport through the equator and that the correlation between seasonal variations of net surface heating and ocean heat storage was poor. Our results do not support their conclusion in the northeastern Indian Ocean, as the correlation is significant there.

Figure 5b shows that the correlation between monthly dT_S/dt and F_{SW} increases poleward and is generally very high, ~0.8–0.9 poleward of 10°, but the correlation within ~10° of the equator is weak, ranging from –0.2 to 0.6. Thus, the seasonal variations of dT_S/dt and F_{SW} are significantly correlated at a confidence level of ~95%, except for the equatorial region. The correlation between monthly dT_S/dt and $-F_{LH}$ is shown in Fig. 6c. Comparing Figs. 6b and 6c, it can be seen that dT_S/dt has a higher correlation with F_{SW} than $-F_{LH}$, except for the western equatorial Pacific ~5°N–5°S, 150°E–170°W. In this equatorial region, the correlation between dT_S/dt and F_{NET} follows closely the correlation between dT_S/dt and $-F_{LH}$. It is noted that the seasonal variations of dT_S/dt, F_{SW}, and F_{NET} are small in the equatorial area (Figs. 3, and 4). This and large solar radiation penetrating through shallow oceanic mixed layer cause F_{SW} and F_{NET} to have low correlation with dT_S/dt near the equator (Anderson et al. 1996; Sui et al. 1997; Godfrey et al. 1998; Chou et al. 2000; and others).

5. Comparison between 1997–98 El Nino and 1998–99 La Nina

The central and eastern equatorial Pacific warms significantly during May 1997–May 1998 corresponding to a strong El Nino, but cools slightly during July 1998–March 2001 corresponding

to a moderate La Nina (Bell et al. 1999, 2000). We focus on the differences of surface heating related parameters between these two events for the boreal winter of October–March (Figs. 6 and 7). To understand the changes in SST and atmospheric circulation over the tropical Pacific and Indian Oceans, the El Nino–La Nina differences in SST, OLR, zonal wind stress and surface wind speed are shown in Fig. 6 for a large domain of 30°S–30°N, 40°E–120°W. Compared to the La Nina, the SST during the El Nino increases by ~2–5°C in the central and eastern equatorial Pacific and by ~1°C in the western equatorial Indian Ocean, but decreases by <1°C near the maritime continent (Fig. 6a). Correspondingly, the maritime continent decreases the deep convective cloudiness indicating by 20–40 W m^{-2} increase in OLR, while the central equatorial Pacific and the western equatorial Indian Ocean increase cloudiness with 40–60 and 20 W m^{-2} decreases in OLR, respectively (Fig. 6b). Thus the Walker circulation weakens in both the tropical Pacific and Indian Oceans during the El Nino as indicated by the changes in OLR and zonal wind stress (Figs. 6b and 6c). Compared to the La Nina, the zonal wind stress during the El Nino increases (more westerly as trade winds weaken) east of ~150°E but decreases (more easterly as trade winds strengthen) west of ~150°E in the equatorial region. The reverse situation is true for the subtropical regions of the south Indian Ocean, southwestern Pacific (resulting in the northward shift of the SPCZ), and northwest Pacific near the northern section of the South China Sea. This is a result of the equatorward shift of trade-wind belts during the El Nino (Yu and Riennecker 2000). Thus, compared to the La Nina, the surface wind speed generally decreases by ~1 m s^{-1} during the El Nino, except for the regions extending from the southern section of the South China Sea to the maritime continent and further to the SPCZ where cloudiness decreases (Fig. 6d).

It is noted that the stronger easterly zonal wind stress near the equator during the El Nino can cause upwelling (downwelling) in the eastern (western) equatorial Indian Ocean. This is related to the Indian Ocean dipole mode and has been extensively discussed by various scientists (e.g., Webster et al. 1999; Saji et al. 1999; Yu and Riennecker 2000; and others). The change of zonal wind stress in the Indian Ocean can increase the oceanic heat transport from the South to the North Indian Ocean during the El Nino as compared to the La Nina (e. g., Loschnigg and Webster 2000).

The change of the zonal wind stress corresponds to relaxed trade winds in the equatorial Pacific during the El Nino. This can reduce the pressure gradient from the Pacific to Indian Ocean across the Indonesia, and, hence, weakens the Indonesian throughflow for transporting heat from the Pacific to Indian Ocean (e.g., Godfrey 1996; Lukas et al. 1996; Meyers 1996). It is generally recognized that a reduced surface wind speed can shallow the oceanic mixed layer and, hence, enhance solar radiation penetrating through the mixed layer (e.g., Anderson et al. 1996; Sui et al. 1997; Godfrey et al. 1998; Chou et al. 2000; and others). The interannual variability of wind stress is thus expected to have significant effect on the mixed-layer heat budget and SST variations in this climatic important region, through the changes not only in the surface heat fluxes but also in the ocean dynamics.

Figure 7 shows the El Nino–La Nina differences in F_{SW}, F_{LH}, F_{NET}, and dT_S/dt, respectively, for the small domain of 30°S–30°N, 90°E–170°W. In accordance with the change in cloudiness, F_{SW} decreases in the equatorial central Pacific but increases in the rest of the domain, whereas the change of F_{LH} follows primarily that of the surface wind and secondarily Q_S–Q_a (Figs. 6b, 6d, 7a, and 7b). The spatial variation of F_{LH} change is much greater than that of F_{SW} change, and, hence, dominates that of F_{NET} change. The domination of F_{NET} change by F_{LH} change over some regions, where the change of F_{NET} between El Nino and La Nina is large, is demonstrated in Table 3 in addition to Fig. 7a-c. In the central equatorial Pacific, the cloudiness increases but wind decreases during the El Nino. Correspondingly, both F_{SW} and F_{LH} decrease with increasing SST, which is consistent with results found by Liu et al. (1994) and Zhang and McPhaden (1995). The decrease of F_{LH} surpasses the decrease of F_{SW}, leading to an increase of F_{NET}. So, the enhancement of convection and cloudiness in the central equatorial Pacific associated with a higher SST leads to an enhancement of surface heating, with a maximum of 40 W m^{-2} at 7°S, 180°E. This is in variance with the hypotheses of SST regulation in the Pacific warm pool that either by the reduced solar heating in response to an enhanced cloudiness (Ramanathan and Collins 1991) or by an enhanced evaporative cooling due to increased SST (Wallace 1992).

Compared to the La Nina, the southern section of SPCZ is less cloudy, more windy, and dryer (greater $Q_s - Q_a$) during the El Nino as the SPCZ shifts northward. The first factor enhances the solar heating, but last two factors enhance the evaporative cooling. The evaporative cooling exceeds the solar heating, resulting in a net surface cooling. The region of a reduced F_{NET} covers a large area with a maximum of –70 W m^{-2}. In the South China Sea (SCS), the F_{SW} change is positive but the F_{LH} change is of opposite signs between the northern and southern sections of SCS. The change of F_{NET} is large in both the northern and southern sections but with opposite signs, following F_{LH} change. The maximum heating in the northern section of the SCS and the maximum cooling in the southern section of the SCS are both ~ 50 W m^{-2}. In the eastern Indian Ocean, the F_{NET} change also follows the patterns of F_{LH} change. The large changes of F_{NET} in the southeastern Indian Ocean, ~110 W m^{-2}, and the eastern equatorial Indian Ocean, ~90 W m^{-2}, are due to a large change of F_{LH} associated with a large reduction in wind speed and the sea-air humidity difference.

It is worth to note that the change of F_{NET} between 1997–98 El Nino and 1998–99 La Nina is significantly larger in the tropical eastern Indian Ocean than tropical western Pacific (Fig. 7 and Table 3). For the eastern Indian Ocean, the reduced evaporative cooling arising from weakened winds during the El Nino is generally associated with enhanced solar heating due to decreased cloudiness, and thus increases the interannual variability of F_{NET}. For the western Pacific, the reduced evaporative cooling due to weakened winds is generally associated with but exceeds the reduced solar heating arising from increased cloudiness, and vise versa. Thus the interannual variability of F_{NET} is reduced due to this offsetting effect.

The change in dT_S/dt is generally larger in the eastern Indian Ocean than the western Pacific, but the interannual variations of F_{NET} and dT_S/dt have very low correlation (Figs. 7c and 7d). In particular, the strong dipole-like change of F_{NET} in the southern equatorial Pacific and the South China Sea are not consistent with the much smoother change of dT_S/dt. Similarly, the broad and strong positive change of dT_S/dt in the eastern Indian Ocean and the maritime continent region is not consistent with the change of F_{NET}, which has a larger spatial variability than the change of dT_S/dt. These results strongly indicate that the change of dT_S/dt during the El Nino is induced by

the change in ocean dynamics but not the surface heating. The change in ocean dynamics includes the interannual variability of solar radiation penetrating through oceanic mixed layer, upwelling of cold thermocline water, Indonesian throughflow for transporting heat from the Pacific to Indian Ocean, and interhemispheric transport in the Indian Ocean. This is generally consistent with the finding of Wang and McPhaden (2001) that all terms in the balance of the oceanic mixed layer contributed to the SST variation during the 1997–98 El Nino and 1998–99 La Nina.

6. Concluding remarks

Seasonal and interannual variations of the net surface heating (F_{NET}) and SST tendency (dT_S/dt) in the tropical eastern Indian and western Pacific Oceans (30°S–30°N, 90°E–170°W) are studied for the 3-yr period October 1997–September 2000. Latent heat flux, sensible heat flux, wind speed, and surface air humidity are derived from the SSM/I radiance measurements, solar and IR fluxes are derived from Japanese GMS radiance measurements, and SST is taken from the NCEP/NCAR reanalysis.

It is found that the magnitude of solar heating (F_{SW}) is lager than that of evaporative cooling (F_{LH}) but the spatial variation of the latter is significantly large than the former. The range of the annual-mean is 180–250 W m^{-2} for F_{SW} and 75–190 W m^{-2} for F_{LH}. As a result, the spatial variations of seasonal and interannual variability of F_{NET} follows closely that of F_{LH}. Seasonal variations of F_{NET} and dT_S/dt are significantly correlated in the region, except for the equatorial western Pacific. The high correlation is primarily attributable to high correlation between seasonal cycles of solar heating and dT_S/dt. In the equatorial region, winds are weak, the oceanic mixed layer is shallow, and the solar radiation penetrating through the mixed layer is significant. Therefore, the relation between F_{NET} and dT_S/dt is weak. In the southeastern Indian Ocean west of Australia, F_{NET} is negative in all seasons, indicating a significant heat convergence within the mixed layer. The Indonesian throughflow transporting heat from the Pacific to Indian Ocean likely plays an important role (Masumoto and Yamagata 1996).

The change of F_{NET} between 1997–98 El Nino and 1998–99 La Nina is significantly larger in the tropical eastern Indian Ocean than tropical western Pacific. For the eastern Indian Ocean, the

reduced evaporative cooling arising from weakened winds during the El Nino is generally associated with enhanced solar heating due to decreased cloudiness, and thus increases the interannual variability of F_{NET}. For the western Pacific, the reduced evaporative cooling due to weakened winds is generally associated with but exceeds the reduced solar heating arising from increased cloudiness, and vise versa. Thus the interannual variability of F_{NET} is reduced due to this offsetting effect. The change in dT_S/dt is generally larger in the eastern Indian Ocean than the western Pacific, but the interannual variations of F_{NET} and dT_S/dt have very low correlation. This is most likely related to interannual variability of ocean dynamics, which includes the variations of solar radiation penetrating through oceanic mixed layer, upwelling of cold thermocline water, Indonesian throughflow for transporting heat from the Pacific to Indian Ocean, and interhemispheric transport in the Indian Ocean. The interannual variability of wind stress is expected to have significant effect on the mixed-layer heat budget and SST variations in this climatic important region, through the changes not only in the surface heat fluxes but also in the ocean dynamics.

Acknowledgments This study was supported by the TRMM Program, Global Modeling and Analysis Program, and Radiation Research Program, NASA/Office of Earth Science. The SSM/I data of total precipitable water, wind speeds, and antenna temperatures were provided by F. Wentz through the website http://www.ssmi.com. Daily SST's and surface air temperatures were obtained from the NCEP/NCAR reanalysis. Hourly turbulent fluxes measured by research ships were provided by C. Fairall of the NOAA/ETL through the SEAFLUX website http://paos.colorado.edu/~curryja/ocean/index.html. Daily GSSTF2 air-sea turbulent fluxes were processed by E. Nelkin and J. Ardizzone.

REFERENCES

Anderson, S. P., R. A. Weller, and R. B. Lukas, 1966: Surface buoyancy forcing and the mixed layer of the western Pacific warm pool: observations and 1D model results. *J. Climate,* **9**, 3056-3085.

Atlas, R., R. N. Hoffman, S. C. Bloom, J. C. Jusem, and J. Ardizzone, 1996: A multiyear global surface wind velocity dataset using SSM/I wind observations. *Bull. Amer. Meteor. Soc.*, **77**, 869-882.

Bell, G. D., and co-authors, 1999: Climate assessment for 1998. *Bull. Amer. Meteor. Soc.*, **80**, S1–S48.

Bell, G. D., and co-authors, 2000: Climate assessment for 1999. *Bull. Amer. Meteor. Soc.*, **81**, S1–S50.

Chou, M.-D., P.-K. Chan, and M. M.-H. Yan, 2001: A sea surface radiation dataset for climate applications in the tropical western Pacific and South China Sea. *J. Geophys. Res.*, **106**, 7219-7228.

Chou, S.-H., R. M. Atlas, C.-L. Shie and J. Ardizzone, 1995: Estimates of surface humidity and latent heat fluxes over oceans from SSM/I data. *Mon. Wea. Rev.*, **123**, 2405-2425.

Chou, S.-H., C.-L. Shie, R. M. Atlas and J. Ardizzone, 1997: Air-sea fluxes retrieved from Special Sensor Microwave Imager data. *J. Geophys. Res.,* **102**, 12705-12726.

Chou, S.-H., W. Zhao, and M.-D. Chou, 2000: Surface heat budgets and sea surface temperature in the Pacific warm pool during TOGA COARE. *J. Climate,* **13**, 634-649.

Chou, S.-H., E. Nelkin, J. Ardizzone, R. M. Atlas, and C.-L. Shie, 2002: Version 2 Goddard Satellite-Based Surface Turbulent Fluxes (GSSTF2). *J. Climate*, (submitted).

da Silva, A, C. C. Young and S. Levitus, 1994: Atlas of Surface Marine Data 1994 Vol. 1: Algorithms and Procedures. NOAA Atlas NESDIS 6, US Dept. of Commerce, NOAA, NESDIS, Washington, DC, 83 pp.

Fairall, C. W., E. F. Bradley, D. P. Rogers, J. B. Edson, and G. S. Young, 1996: Bulk parameterization of air-sea fluxes for Tropical Ocean Global Atmosphere Coupled Ocean-Atmosphere Response Experiment. *J. Geophys. Res.*, **101**, 3747-3764.

Godfrey, J. S, 1996: The effect of the Indonesian throughflow on ocean circulation and heat exchange with the atmosphere: A review. *J. Geophy. Res.*, **101**, 12217-12237.

Godfrey, J. S., R. A. House Jr., R. H. Johnson, R. Lukas, J.-L. Redelsperger, A. Sumi, and R. Weller, 1998: Coupled Ocean-Atmosphere Response Experiment (COARE): An interim report. *J. Geophy. Res.*, **103**, 14395-14450.

Kalnay, E., and co-authors, 1996: The NCEP/NCAR 40-year reanalysis project. *Bull. Amer. Meteor. Soc.*, **77**, 437-471.

Kubota, M., K. Ichikawa, N. Iwasaka, S. Kizu, M. Konda, and K. Kutsuwada, 2002: Japanese Ocean Flux Data Sets with Use of Remote Sensing Observations (J-OFURO) introducing J-OFURO. *J. Oceanog.*, **58**, 213-215.

Lau, K.-M., and P. H. Chan, 1983: Short term climate variability and atmospheric teleconnection from satellite observed outgoing longwave radiation. Part II: Lagged correlations. *J. Atmos. Sci.*, **40**, 2751-2767.

Liu, W. T., J. Zhang, and J. K. B. Bishop, 1994: Evaporation and solar irradiance as regulators of sea surface temperature in annual and interannual changes. *J. Geophys. Res.*, **99**, 12623-12637.

Loschnigg, J., and P. Webster, 2000: A coupled ocean-atmosphere system of SST modulation for the Indian Ocean. *J. Climate*, **13**, 3342-3360.

Lukas, R, T. Yamagata, and J. P. McCreary, 1996: Pacific low-latitude western boundary currents and the Indonesian throughflow. *J. Geophy. Res.*, **101**, 12209-12216.

Masumoto, Y. and T. Yamagata, 1996: Seasonal variations of the Indonesian throughflow in a general ocean circulation model. *J. Geophy. Res.*, **101**, 12287-12293.

Meyers, G., 1996: Variation of Indonesian throughflow and the El Nino-Southern Oscillation. *J. Geophy. Res.*, **101**, 12255-12263.

Oberhuber, J. M., 1988: *An Atlas Based on the COADS Data Set: The Budgets of Heat, Buoyancy, and Turbulence Kinetic Energy at the Surface of the Global Ocean.* Rep. No. 15, Max-Planck Inst. for Meteorol., Hamburg, Germany.

Palmer, T. N., and D. A., Mansfield, 1984: Response of two atmospheric general circulation models to sea-surface temperature anomalies in the tropical east and west Pacific. *Nature*, **310**, 483-485.

Ramanathan, V., and W. Collins, 1991: Thermodynamic regulation of ocean warming by cirrus clouds deduced from observations of the 1987 El Nino. *Nature*, **351**, 27-32.

Saji, N. N., B. N. Goswami, P. N. Vinayachandran, and T. Yamagata, 1999: A dipole mode in the tropical Indian Ocean. *Nature*, **401**, 360-363.

Sui, C.-H., X. Li, K.-M. Lau, and D. Adamac, 1997: Mutiscale air-sea interactions during TOGA COARE. *Mon. Wea. Rev.*, **125**, 448-462.

Wallace, J. M., 1992: Effect of deep convection on the regulation of tropical sea surface temperature. *Nature*, **357**, 230-231.

Wang, W., and M. J. McPhaden, 2001: Surface layer temperature balance in the equatorial Pacific during the 1997-98 El Nino and 1998-99 La Nina. *J. Climate*, **14**, 3393-3407.

Webster, P. J., A. Moore, J. Loschnigg, and R. Leben, 1999: Coupled ocean–atmosphere dynamics in the Indian Ocean during 1997-1998. *Nature*, **401**, 356-360.

Webster, P. J., T. Palmer, M. Yanai, V. Magana, J. Shukla, R. A. Toma, and A. Yasunari, 1998: Monsoons: Processes, Predicability and the prospects for prediction. *J. Geophys. Res.*, **103**, (C7), 14451-14510.

Webster, P. J. and co-authors, 2002: The JASMINE pilot study. *Bull. Amer. Meteor. Soc.*, **83**, 1603-1630.

Wentz, F. J., 1997: A well calibrated ocean algorithm for SSM/I. *J. Geophys. Res.*, **102**, 8703-8718.

Yu, L., and M. Rienecker, 2000: Indian Ocean warming of 1997-98. *J. Geophys. Res.*, **105**, 16923-16939.

Zhang, G. J., and M. J. McPhaden, 1995: The relationship between sea surface temperature and latent heat flux in the equatorial Pacific. *J. Climate*, **8**, 589-605.

TABLE 1. The periods and locations of five tropical field experiments conducted by the NOAA/ETL research ships.

Experiments	Periods	Locations
ASTEX	92/6/6–92/6/28	30°N, 36°W
COARE	92/11/11–93/2/16	1.7°S, 156°E
JASMINE	99/5/4–99/5/31	5°S–13°N, 88–98°E
KWAJEX	99/7/28–99/9/10	9°N, 167°E
NAURU99	99/6/15–99/7/18	12°S, 130°E–8°N, 167°E

Table 2. Comparison of daily latent heat fluxes (F_{LH}), sensible heat fluxes (F_{SH}), wind stress, surface wind speed (U), surface air humidity (Q_a), surface air temperature (T_a), and SST of GSSTF2 with those measured by ships during the five tropical field experiments. The mean is the ship-observed values averaged over 134 days of collocation, positive bias indicates larger GSSTF2, SD error is the standard deviation error, and r is the correlation coefficient.

Variable	Unit	Mean	Bias	SD error		r
				Daily	Monthly	
F_{LH}	W m^{-2}	93.0	–2.6	29.7	5.4	0.80
F_{SH}	W m^{-2}	5.5	7.0	6.2	1.1	0.45
stress	10^{-3} N m^{-2}	32.7	5.3	19.3	3.5	0.81
U	m s^{-1}	4.5	0.34	1.12	0.20	0.85
Q_a	g kg^{-1}	17.8	1.01	1.10	0.20	0.85
T_a	°C	27.4	–0.83	0.73	0.13	0.94
SST	°C	28.5	–0.01	0.31	0.06	0.99

Table 3. El Nino–La Nina differences in the surface heating between 1997–98 El Nino and 1998–99 La Nina. Fluxes are averaged over the boreal winter of October-March. F_{SW}, F_{LH}, and F_{NET} are solar heating, evaporative cooling, and net surface heating, respectively. Units are W m^{-2}.

	ΔF_{SW}	ΔF_{LH}	ΔF_{NET}
Central equatorial Pacific (7°S, 180°E)	–43	–65	40
Southern SPCZ (20°S, 176°W)	17	73	–69
Northern SCS (20°N, 120°E)	24	–32	52
Southern SCS (6°N, 110°E)	38	69	-48
Southeastern Indian Ocean (20°S, 92°E)	26	–72	108
Eastern equatorial Indian Ocean (0°, 92°E)	36	–49	89

FIGURE CAPTIONS

Fig. 1. Surface (a) solar heating , (b) IR cooling, (c) evaporative cooling, and (d) net heating, averaged over the 3-yr period October 1997–September 2000.

Fig. 2. (a) OLR, (b) SST, (c) sea–air humidity difference, and (d) 10-m wind speed, averaged over the 3-yr period October 1997–September 2000.

Fig. 3. Seasonal-mean net surface heating for the boreal (a) winter, DJF, (b) spring, MAM, (c) summer, JJA, and (d) fall, SON, of October 1997–September 2000.

Fig. 4. Same as Fig.3, except for the SST tendency.

Fig. 5. Correlation coefficients of monthly SST tendency and monthly (a) net surface heating, (b) solar heating, and (c) evaporative heating for the 3-yr period October1997–September 2000. Shaded areas indicate correlation significant at the 95% level.

Fig. 6. 1997/98 El Nino–1998/99 La Nina differences of (a) SST, (b) OLR, (c) zonal wind stress, and (d) 10-m wind speed for the boreal winter of October–March.

Fig. 7. Same as Fig. 6, except for (a) solar heating, (b) evaporative cooling, (c) net surface heating, and (d) SST tendency.

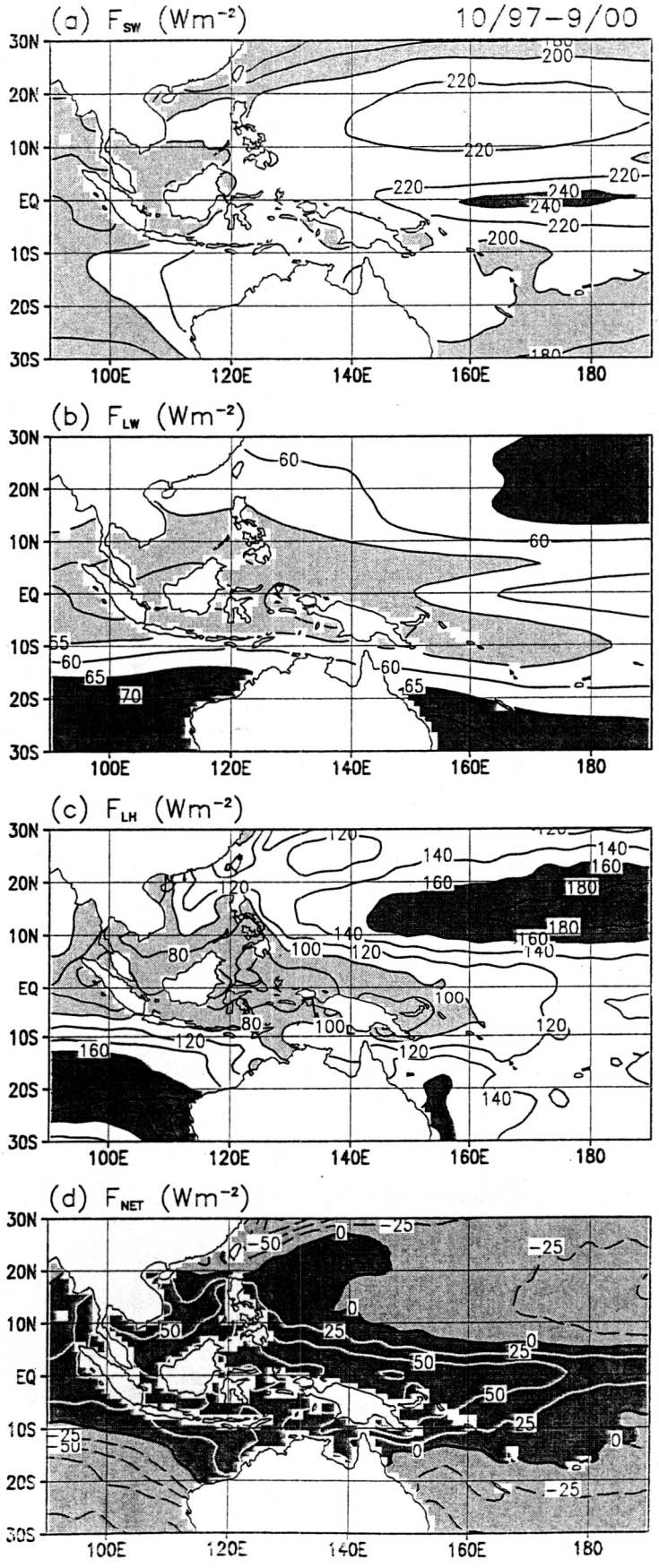
(a) F_{SW} (Wm^{-2})
10/97–9/00
(b) F_{LW} (Wm^{-2})
(c) F_{LH} (Wm^{-2})
(d) F_{NET} (Wm^{-2})
30N
20N
10N
EQ
10S
20S
30S
100E
120E
140E
160E
180

Fig. 1

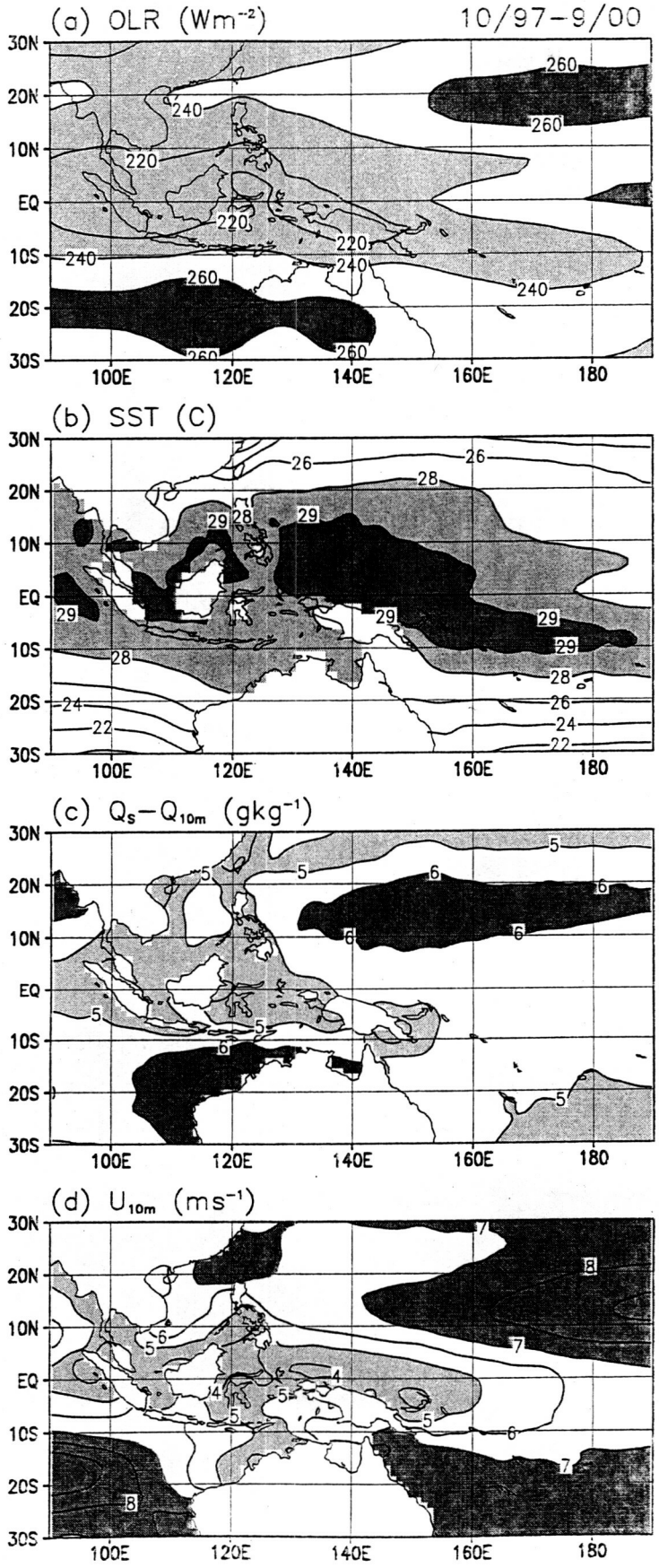
(a) OLR (Wm⁻²)
10/97-9/00
(b) SST (C)
(c) Qs−Q10m (gkg⁻¹)
(d) U10m (ms⁻¹)
30N
20N
10N
EQ
10S
20S
30S
100E
120E
140E
160E
180

Fig. 2

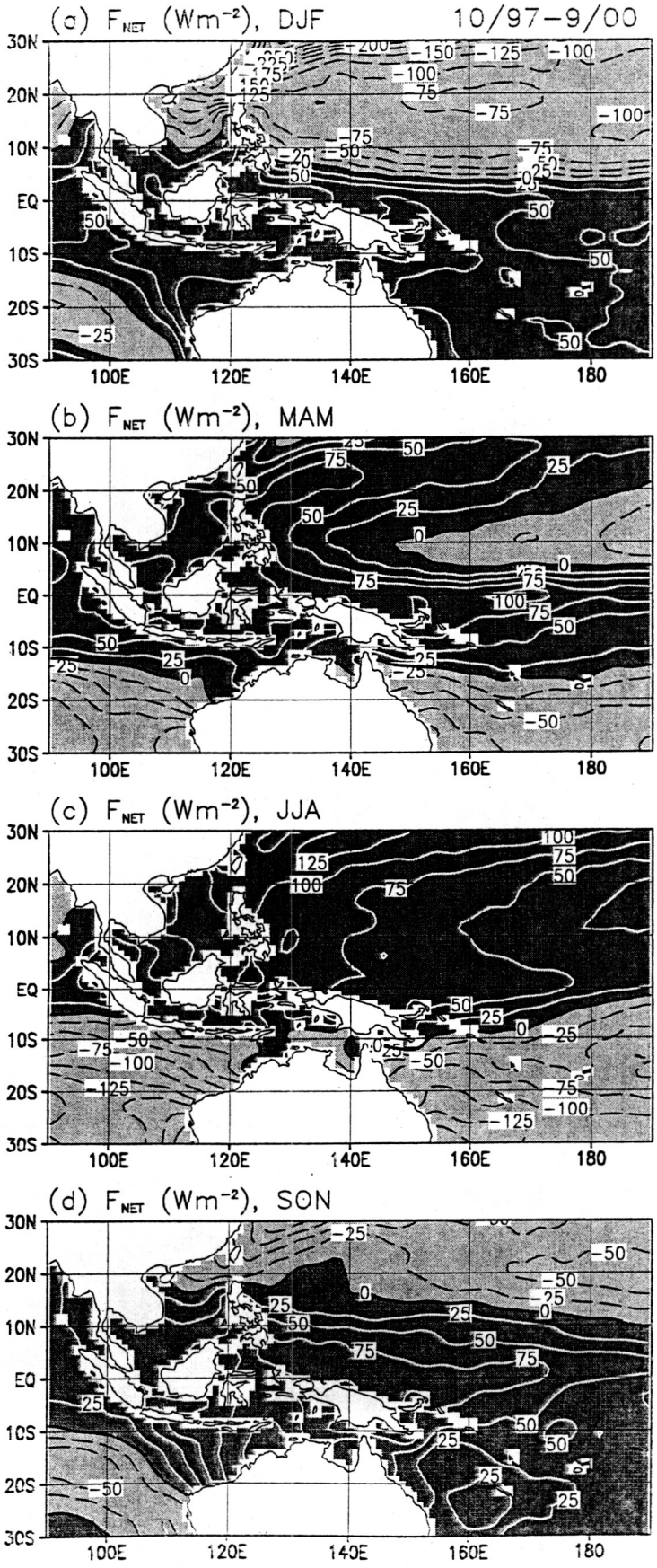
(a) F_{NET} (Wm^{-2}), DJF 10/97–9/00
(b) F_{NET} (Wm^{-2}), MAM
(c) F_{NET} (Wm^{-2}), JJA
(d) F_{NET} (Wm^{-2}), SON
30N
20N
10N
EQ
10S
20S
30S
100E
120E
140E
160E
180

Fig. 3

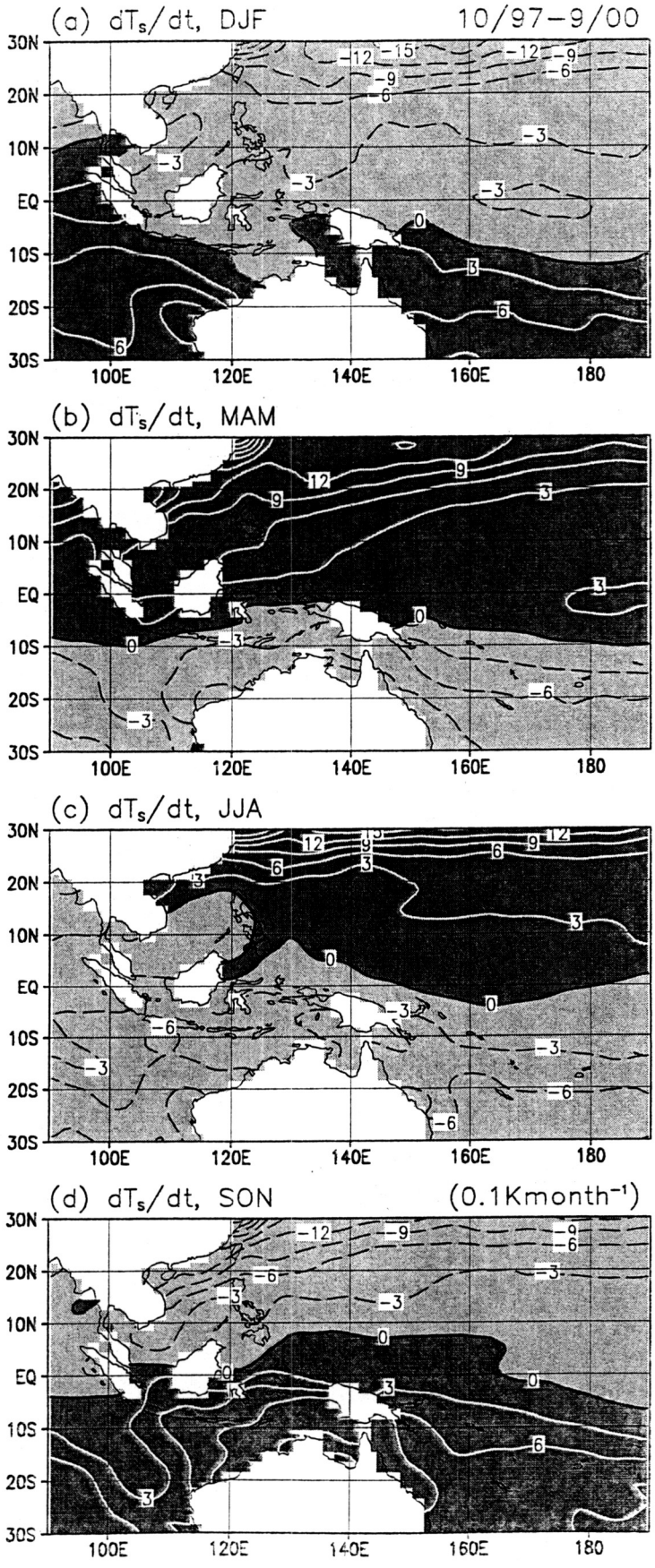
(a) dTs/dt, DJF
10/97–9/00
(b) dTs/dt, MAM
(c) dTs/dt, JJA
(d) dTs/dt, SON
(0.1Kmonth⁻¹)
30N
20N
10N
EQ
10S
20S
30S
100E
120E
140E
160E
180

Fig. 4

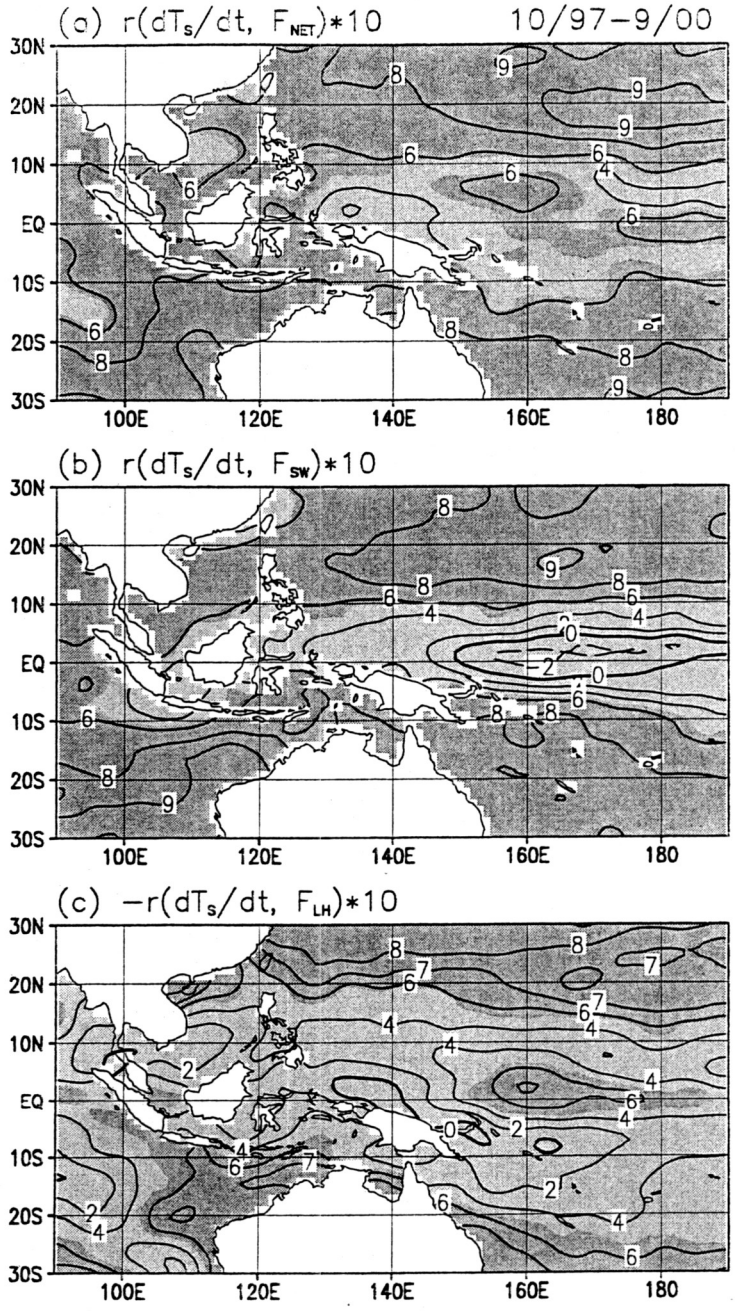
(a) r(dTs/dt, FNET)*10
10/97–9/00
(b) r(dTs/dt, FSW)*10
(c) −r(dTs/dt, FLH)*10
30N
20N
10N
EQ
10S
20S
30S
100E
120E
140E
160E
180

Fig. 5

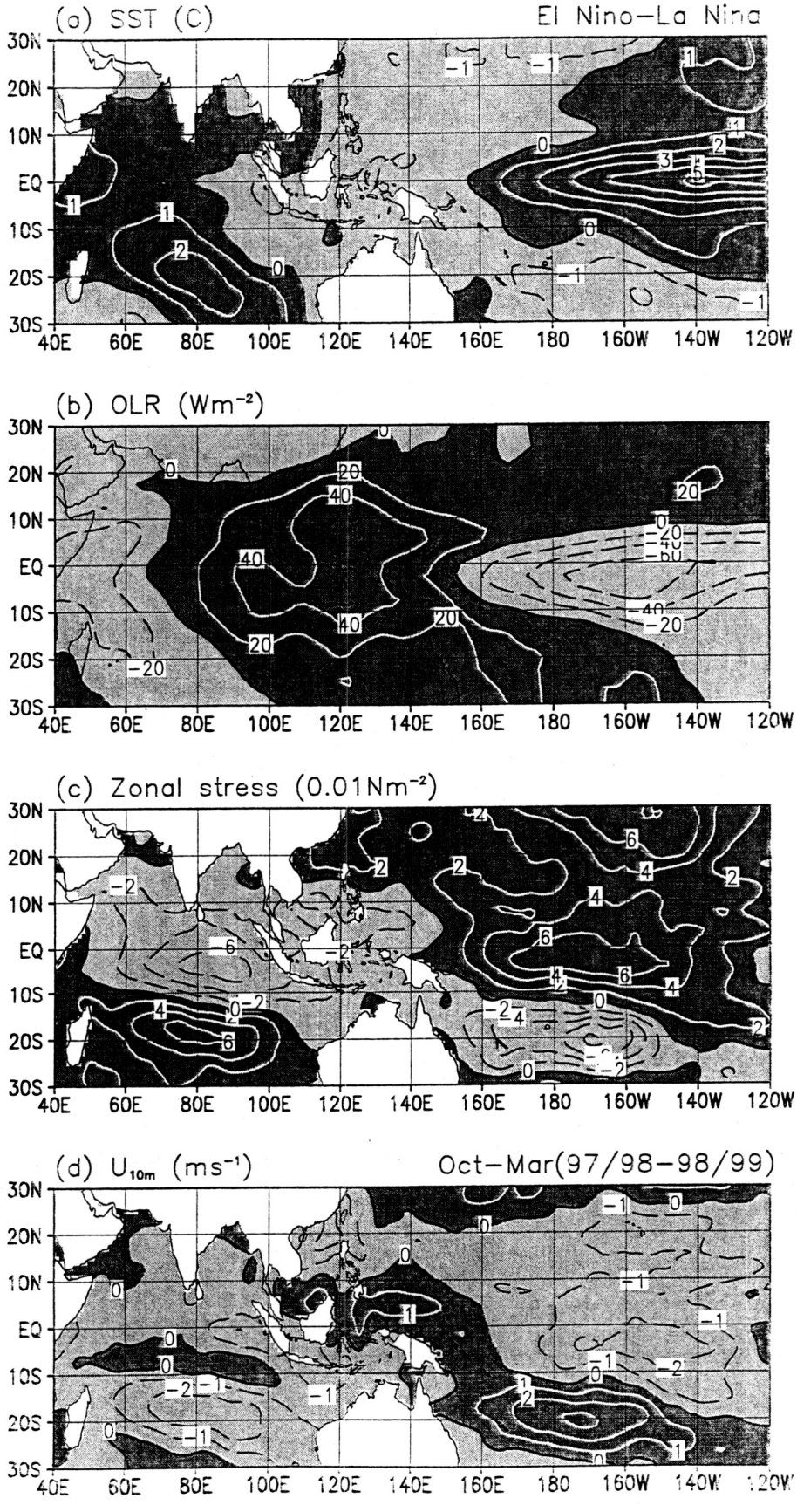
(a) SST (C)
El Nino–La Nina
(b) OLR (Wm⁻²)
(c) Zonal stress (0.01Nm⁻²)
(d) U10m (ms⁻¹)
Oct–Mar(97/98–98/99)
30N
20N
10N
EQ
10S
20S
30S
40E
60E
80E
100E
120E
140E
160E
180
160W
140W
120W

Fig. 6

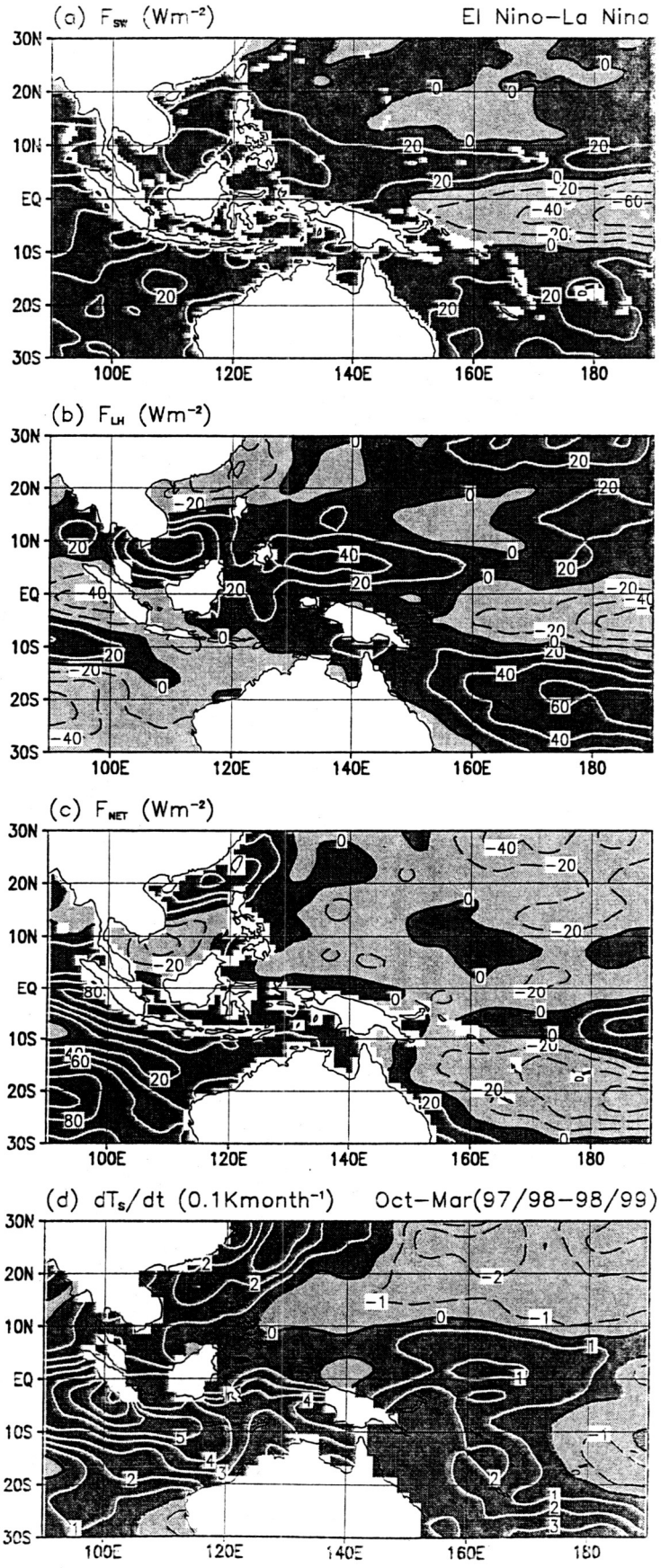
(a) F_{SW} (Wm^{-2})
El Nino–La Nina
(b) F_{LH} (Wm^{-2})
(c) F_{NET} (Wm^{-2})
(d) dT_s/dt (0.1Kmonth^{-1})
Oct–Mar(97/98–98/99)
30N
20N
10N
EQ
10S
20S
30S
100E
120E
140E
160E
180

Fig.7

Tropical Warm Pool Surface Heat Budgets and Temperature: Contrasts Between 1997–98 El Nino and 1998–99 La Nina

Shu-Hsien Chou, Ming-Dah Chou, Pui-King Chan, Po-Hsiung Lin, and Kung-Hwa Wang

Popular Summary

Seasonal and interannual variations of surface heat budgets and sea surface temperature (SST) tendency in the tropical eastern Indian and western Pacific Oceans are studied. The surface heat fluxes are derived from the Special Sensor Microwave/Imager and Japanese Geostationary Meteorological Satellite radiance measurements for the period October 1997–September 2000. The period includes the 1997–98 strong El Nino and the 1998–99 moderate La Nina. It is found that the magnitude of solar heating is lager than that of evaporative cooling, but the spatial variation of the latter is significantly large than the former. As a result, the spatial variations of seasonal and interannual variability of the net surface heating follow closely that of evaporative cooling.

The change of net surface heating between 1997–98 El Nino and 1998–99 La Nina is significantly larger in the tropical eastern Indian Ocean than tropical western Pacific. For the former region, the reduced evaporative cooling arising from weakened winds during the El Nino is generally associated with enhanced solar heating due to decreased cloudiness, and thus increases the interannual variability of net surface heating. For the latter region, the reduced evaporative cooling due to weakened winds is generally associated with but exceeds the reduced solar heating arising from increased cloudiness, and vise versa. Thus the interannual variability of net surface heating is reduced due to this offsetting effect. Interannual variations of net surface heating and SST tendency have very low correlation. This is most likely related to interannual variability of ocean dynamics, which includes the variations of solar radiation penetrating through oceanic mixed layer, upwelling of cold thermocline water, Indonesian throughflow for transporting heat from the Pacific to Indian Ocean, and interhemispheric transport in the Indian Ocean.

Shu-Hsien Chou and Ming-Dah Chou, Laboratory for Atmospheres, NASA/Goddard Space Flight Center, Greenbelt, MD 20771

Pui-King Chan, Science Systems & Applications, Inc., Lanham, MD 20706

Po-Hsiung Lin, National Taiwan University, Taipei, Taiwan

Kung-Hwa Wang, Central Weather Bureau, Taipei, Taiwan